Fission barriers in covariant density functional theory: Extrapolation to superheavy nuclei

H. Abusara,[1,2] A. V. Afanasjev,[1] and P. Ring[3]

[1]*Department of Physics and Astronomy, Mississippi State University, Mississippi 39762, USA*
[2]*Department of Electronics and Applied Physics, Palestine Polytechnic University, 705 Hebron, Palestinian territory*
[3]*Fakultät für Physik, Technische Universität München, D-85748 Garching, Germany*

Systematic calculations of fission barriers allowing for triaxial deformation are performed for even-even superheavy nuclei with charge number $Z = 112$–120 using three classes of covariant density functional models. The softness of nuclei in the triaxial plane leads to an emergence of several competing fission paths in the region of the inner fission barrier in some of these nuclei. The outer fission barriers are considerably affected by triaxiality and octupole deformation. General trends of the evolution of the inner and the outer fission barrier heights are discussed as a function of the particle numbers.

I. INTRODUCTION

The ongoing search for new superheavy elements is motivated by the attempts to provide theoretical and experimental explanations for two open questions in nuclear structure. The first question is related to the limits of the existence of atomic nuclei at large values of proton number, while the second one is related to the location of the island of stability of superheavy nuclei and the next magic numbers (if any) beyond $Z = 82$ and $N = 126$. Heavy and superheavy nuclei decay by spontaneous fission and therefore their stability is defined essentially by the size and the shape of the fission barriers. Thus, the inner fission barrier is considered a fundamental characteristic of these nuclei which is important in resolving the questions mentioned above.

A systematic investigation of the properties of fission barriers is the best way to address the stability of nuclei against spontaneous fission since it eliminates the arbitrariness of conclusions with respect to the choice of a specific nucleus. Different models with triaxiality included have been used for extensive theoretical investigations of the properties of inner fission barriers in the actinides. It has been found that the heights of inner fission barriers are reduced when triaxial shapes are taken into account [1–3]. However, this reduction has a strong dependence on the particle number in the proton and neutron subsystems as well as on the applied model. These investigations were performed in the following frameworks: microscopic + macroscopic (MM) methods [4–9], the extended Thomas-Fermi plus Strutinsky integral (ETFSI) method [10], nonrelativistic energy density functionals (EDF) based on zero-range Skyrme [2,11–13] and finite-range Gogny [3,14–16] forces, and recently in covariant density functional theory (CDFT) [1,17,18].

These methods have also been used for the study of fission barriers in superheavy nuclei (see Table IV below for a review). However, only a few of them take into account triaxiality. For example, within the framework of covariant density functional theory, it has been considered only in the study of fission barriers in a single nucleus (^{264}Hs) in Ref. [11]. Thus, in order to fill this gap in our knowledge, a systematic study of fission barriers of even-even $Z = 112$–120 superheavy nuclei

with triaxiality included is performed in the current paper. We use the same method that has been successfully employed in Ref. [1] for the study of inner fission barriers in actinides, where an average deviation from experiment of 0.76 MeV has been found. When extrapolating to superheavy nuclei we want to understand the impact of triaxiality on fission barriers and how they evolve with the change of the particle numbers. An additional goal is to see how the fission barriers depend on the choice of the specific CDFT model. While the systematic investigation of inner fission barriers of actinides in Ref. [1] has been performed with the nonlinear meson-nucleon coupling model represented by the NL3* parametrization of the relativistic mean-field (RMF) Lagrangian, in the current study we use in addition to the nonlinear coupling model also density-dependent meson-nucleon and point coupling models.

Density functional theories are extremely useful for the microscopic description of quantum mechanical many-body systems. They have been applied with great success for many years in Coulombic systems [19,20], where they are in principle exact and where the functional can be derived without any phenomenological adjustments directly from the Coulomb interaction. In nuclear physics with spin and isospin degrees of freedom, with strong nucleon-nucleon and three-body forces the situation is much more complicated. However, covariant density functionals exploit basic properties of QCD at low energies, in particular symmetries and the separation of scales [21]. They provide a consistent treatment of the spin degrees of freedom, and they include the complicated interplay between the large Lorentz scalar and vector self-energies induced on the QCD level by the in-medium changes of the scalar and vector quark condensates [22]. In addition, these functionals include *nuclear magnetism* [23], i.e., a consistent description of currents and time-odd mean fields important for odd-mass nuclei [24], the excitations with unsaturated spins, magnetic moments [25], and nuclear rotations [26,27]. Because of Lorentz invariance no new adjustable parameters are required for the time-odd parts of the mean fields. Of course, at present, no attempts to derive these functionals directly from the bare forces [28–31] have reached the required accuracy. However, in recent years modern and very successful covariant

density functionals have been derived [32–35]; these are based on density-dependent vertices and one additional parameter characterizing the range of the force. They provide an excellent description of ground states and excited states over the entire periodic table [36,37] with a high predictive power. Modern versions of these forces derive the density dependence of the vertices from state-of-the-art *ab initio* calculations and use only the remaining few parameters for a fine tuning of experimental masses in finite spherical [35] and deformed [34] nuclei.

The paper is organized as follows. The theoretical framework and the details of the numerical calculations are discussed in Sec. II. The results of the investigations of the fission barriers, the role of triaxiality, and the comparison with the actinide region are presented in Sec. III. Finally, Sec. IV summarizes the results of our work.

II. THEORETICAL FRAMEWORK AND THE DETAILS OF THE NUMERICAL CALCULATIONS

Three classes of covariant density functional models are used throughout this paper: the nonlinear meson-nucleon coupling model (NL), the density-dependent meson-exchange model (DD-ME), and a density-dependent point coupling model (DD-PC). The main differences among them lay in the treatment of the range of the interaction, the mesons, and the density dependence. The interaction in the first two classes has a finite range, while the third class uses a zero-range interaction with one additional gradient term in the scalar-isoscalar channel. The mesons are absent in the density-dependent point coupling model. The density dependence is explicit in the last two models, while it shows up via the nonlinearity in the σ meson in the nonlinear meson-nucleon coupling model. Each of these classes is represented here by a set of parameters that is considered to be state of the art.

In the meson-exchange models [33,38,39], the nucleus is described as a system of Dirac nucleons interacting via the exchange of mesons with finite masses, leading to finite-range interactions. The starting point of CDFT for these two models is a standard Lagrangian density [40]

$$
\begin{aligned}
\mathcal{L} = &\ \bar{\psi}[\gamma(i\partial - g_\omega\omega - g_\rho\vec{\rho}\,\vec{\tau} - eA) - m - g_\sigma\sigma]\psi \\
&+ \tfrac{1}{2}(\partial\sigma)^2 - \tfrac{1}{2}m_\sigma^2\sigma^2 - \tfrac{1}{4}\Omega_{\mu\nu}\Omega^{\mu\nu} + \tfrac{1}{2}m_\omega^2\omega^2 \\
&- \tfrac{1}{4}\vec{R}_{\mu\nu}\vec{R}^{\mu\nu} + \tfrac{1}{2}m_\rho^2\vec{\rho}^{\,2} - \tfrac{1}{4}F_{\mu\nu}F^{\mu\nu},
\end{aligned}
\tag{1}
$$

which contains nucleons described by the Dirac spinors ψ with mass m and several effective mesons characterized by the quantum numbers of spin, parity, and isospin. They create effective fields in a Dirac equation, which corresponds to the Kohn-Sham equation [19] in the nonrelativistic case. The Lagrangian (1) contains as parameters the meson masses m_σ, m_ω, and m_ρ and the coupling constants g_σ, g_ω, and g_ρ. e is the charge of the proton and it vanishes for neutrons. This linear model has first been introduced by Walecka [41,42].

To treat the density dependence in this model Boguta and Bodmer [43] introduced a density dependence via a nonlinear

TABLE I. The parameters of the NL3* and DD-ME2 parametrizations of the Lagrangian. Note that $g_\sigma = g_\sigma(\rho_{\rm sat})$, $g_\omega = g_\omega(\rho_{\rm sat})$, and $g_\rho = g_\rho(\rho_{\rm sat})$ in the case of the DD-ME2 parametrization.

Parameter	NL3*	DD-ME2
m	939	939
m_σ	502.5742	550.1238
m_ω	782.600	783.000
m_ρ	763.000	763.000
g_σ	10.0944	10.5396
g_ω	12.8065	13.0189
g_ρ	4.5748	3.6836
g_2	-10.8093	
g_3	-30.1486	
a_σ		1.3881
b_σ		1.0943
c_σ		1.7057
d_σ		0.4421
a_ω		1.3892
b_ω		0.9240
c_ω		1.4620
d_ω		0.4775
a_ρ		0.5647

meson coupling replacing the term $\tfrac{1}{2}m_\sigma^2\sigma^2$ in Eq. (1) by

$$
U(\sigma) = \tfrac{1}{2}m_\sigma^2\sigma^2 + \tfrac{1}{3}g_2\sigma^3 + \tfrac{1}{4}g_3\sigma^4.
\tag{2}
$$

The nonlinear meson-nucleon coupling is represented by the parameter set NL3* [38] (see Table I), which is a modern version of the widely used parameter set NL3 [44]. Apart from the fixed values for the masses m, m_ω, and m_ρ, there are six phenomenological parameters: m_σ, g_σ, g_ω, g_ρ, g_2, and g_3.

The density-dependent meson-nucleon coupling model has an explicit density dependence for the meson-nucleon vertices. There are no nonlinear terms in the σ meson, i.e., $g_2 = g_3 = 0$. The meson-nucleon vertices are defined as

$$
g_i(\rho) = g_i(\rho_{\rm sat})f_i(x) \quad \text{for} \quad i = \sigma, \omega, \rho,
\tag{3}
$$

where the density dependence is given by

$$
f_i(x) = a_i \frac{1 + b_i(x + d_i)^2}{1 + c_i(x + d_i)^2}
\tag{4}
$$

for σ and ω and by

$$
f_\rho(x) = \exp[-a_\rho(x - 1)]
\tag{5}
$$

for the ρ meson. x is defined as the ratio between the baryonic density ρ at a specific location and the baryonic density at saturation, $\rho_{\rm sat}$, in symmetric nuclear matter. The eight parameters in Eq. (4) are not independent but constrained as follows: $f_i(1) = 1$, $f_\sigma''(1) = f_\omega''(1)$, and $f_i''(0) = 0$. These constraints reduce the number of independent parameters for density dependence to three. This model is represented in the present investigations by the parameter set DD-ME2 [33] given in Table I.

TABLE II. The parameters of the DD-PC1 parametrization in the RMF Lagrangian.

Parameter	DD-PC1
m	939
a_σ	-10.04616
b_σ	-9.15042
c_σ	-6.42729
d_σ	1.37235
a_ω	5.91946
b_ω	8.86370
d_ω	0.65835
b_ρ	1.83595
d_ρ	0.64025

TABLE III. The G_1^n, G_2^n, G_1^p, and G_2^p parameters (in MeV) for different parametrizations of the RMF Lagrangian.

Force	G_1^n	G_2^n	G_1^p	G_2^p
NL3*	10.7	-10.4	7.40	18.9
DD-PC1	10.5	-7.38	7.5	19.2
DD-ME2	11.0	-10.3	7.9	17.0

The Lagrangian for the density-dependent point coupling model [34,45] is given by

$$
\begin{aligned}
\mathcal{L} = {}& \bar{\psi}(i\gamma \cdot \partial - m)\psi \\
& - \frac{1}{2}\alpha_S(\hat{\rho})(\bar{\psi}\psi)(\bar{\psi}\psi) - \frac{1}{2}\alpha_V(\hat{\rho})(\bar{\psi}\gamma^\mu\psi)(\bar{\psi}\gamma_\mu\psi) \\
& - \frac{1}{2}\alpha_{TV}(\hat{\rho})(\bar{\psi}\vec{\tau}\gamma^\mu\psi)(\bar{\psi}\vec{\tau}\gamma_\mu\psi) \\
& - \frac{1}{2}\delta_S(\partial_v\bar{\psi}\psi)(\partial^v\bar{\psi}\psi) - e\bar{\psi}\gamma \cdot A\frac{(1-\tau_3)}{2}\psi.
\end{aligned} \tag{6}
$$

It contains the free-nucleon Lagrangian, the point coupling interaction terms, and the coupling of the proton to the electromagnetic field. The derivative terms in Eq. (6) account for the leading effects of finite-range interaction, which are important in nuclei. In analogy with meson-exchange models, this model contains isoscalar-scalar, isoscalar-vector, and isovector-vector interactions. In the present work it is represented by the DD-PC1 parametrization [34] given in Table II.

The triaxial relativistic mean-field (RMF) + BCS approach [46] is used here for the description of fission barriers. This approach has been very successfully applied to a systematic description of the fission barriers in the actinides [1]. The RMF equations are solved iteratively and at each iteration the BCS occupation probabilities v_k^2 are determined. These quantities are used in the calculation of densities, energies, and new fields for the next iteration. We use a monopole pairing force [47] with the strength parameters G_τ for neutrons ($\tau = n$) and protons ($\tau = p$).

For each type of particle we start with a pairing strength parameter G and solve at each iteration the gap equation [47]

$$
\frac{1}{G} = \sum_{k>0}\frac{1}{2E_k} \tag{7}
$$

with $E_k = \sqrt{(\varepsilon_k - \lambda)^2 + \Delta^2}$, where ε_k are the eigenvalues of the Dirac equation and the chemical potential λ is determined by the average particle number. Then the occupation probabilities

$$
v_k^2 = \frac{1}{2}\left(1 - \frac{\varepsilon_k - \lambda}{E_k}\right) \tag{8}
$$

and the gap parameters

$$
\Delta = G\sum_{k>0}u_k v_k \tag{9}
$$

are determined in a self-consistent way. The pairing energy is defined as

$$
E_{\text{pair}} = -\Delta\sum_{k>0}u_k v_k. \tag{10}
$$

The sum over k in Eqs. (7), (9), and (10) runs over all states in the pairing window $E_k < E_{\text{cutoff}}$. In Ref. [48] empirical pairing gap parameters

$$
\Delta_n^{\text{emp}} = \frac{4.8}{N^{1/3}} \quad \text{MeV}, \quad \Delta_p^{\text{emp}} = \frac{4.8}{Z^{1/3}} \quad \text{MeV} \tag{11}
$$

have been determined by a fit to experimental data on neutron and proton gaps in the normal deformed minimum.

These empirical gap parameters form the basis for the definition of the strength parameters G_τ in the current paper. We use the following expressions [50] in the calculations:

$$
A \cdot G_n = G_1^n - G_2^n\frac{N-Z}{A} \quad \text{MeV}, \tag{12}
$$

$$
A \cdot G_p = G_1^p + G_2^p\frac{N-Z}{A} \quad \text{MeV}. \tag{13}
$$

First, by using empirical gap parameters of Eq. (11), the values $G_n(Z, N)$ and $G_p(Z, N)$ are obtained for the ground states of all even-even nuclei in the $Z = 112$–126, $N - Z = 48$–62 region. Then, the parameters G_1^n, G_2^n, G_1^p, and G_2^p are defined by the least-squares fit to the set of the $G_n(Z, N)$ and $G_p(Z, N)$. Their values depend on the parameter set of the Lagrangian and they are given in Table III. In this way we have strength parameters for the effective pairing interaction depending in a smooth way on the neutron and proton numbers and, because of the changing level density, the gap parameters derived from those values show fluctuations as a function of the particle numbers. Note that, similarly to Ref. [1], the cutoff energy for the pairing window is set to $E_{\text{cutoff}} = 120$ MeV.

The calculations are performed by successive diagonalizations using the Broyden method [58] and the method of quadratic constraints [47]. We have also implemented the augmented Lagrangian method [59] for constraints in our computer codes, but we did not find any clear advantage of this method over the method of quadratic constraints for the type of potential energy surfaces (PES) we are dealing with. Starting from the three multipole operators

$$
\hat{Q}_{20} = 2z^2 - x^2 - y^2, \tag{14}
$$

$$
\hat{Q}_{22} = x^2 - y^2, \tag{15}
$$

$$
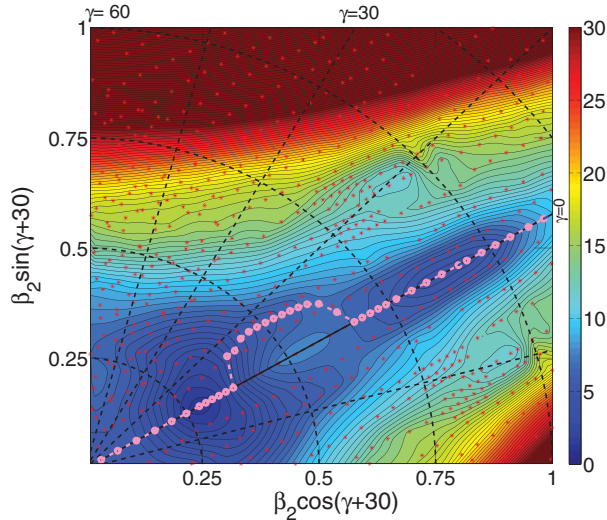\hat{Q}_{30} = z(2z^2 - 3x^2 - 3y^2), \tag{16}
$$

FIG. 1. (Color online) Potential energy surface of the ^{240}Pu nucleus with the NL3* parametrization of the RMF Lagrangian. The energy difference between two neighboring equipotential lines is equal to 0.5 MeV. The pink dashed line with solid circles shows the lowest-energy solution as a function of β_2. Small red stars show the positions of deformation points at which the numerical results were obtained. The figure is based on the results of Ref. [1]. Further details are given in the text.

we calculate in the following investigations three types of potential energy surfaces, using three types of constraints.

First, we restrict ourselves to axially symmetric configurations with reflection symmetry, abbreviated throughout the paper by (A). Here we use the computer code DIZ [60] based on an expansion of the Dirac spinors in terms of harmonic oscillator wave functions with cylindrical symmetry and we minimize

$$\langle H \rangle + C_{20}(\langle \hat{Q}_{20} \rangle - q_{20})^2, \qquad (17)$$

where $\langle H \rangle$ is the total energy, $\langle \hat{Q}_{20} \rangle$ denotes the expectation values of the mass quadrupole operators, q_{20} is the constrained value of the multipole moment, and C_{20} is the corresponding stiffness constant [47].

In the next step, abbreviated throughout the paper by (T), we use the triaxial computer code DIC [23] with the D2 symmetry based on an expansion of the Dirac spinors in terms of a Cartesian oscillator basis and by imposing constraints on axial and triaxial mass quadrupole moments we minimize

$$\langle H \rangle + \sum_{\mu=0,2} C_{2\mu}(\langle \hat{Q}_{2\mu} \rangle - q_{2\mu})^2. \qquad (18)$$

In addition, starting from the axial reflection-symmetric computer code DIZ of Ref. [60], we have developed an axial reflection-asymmetric (octupole deformed) code DOZ. It is used for a study of the impact of axial octupole deformation
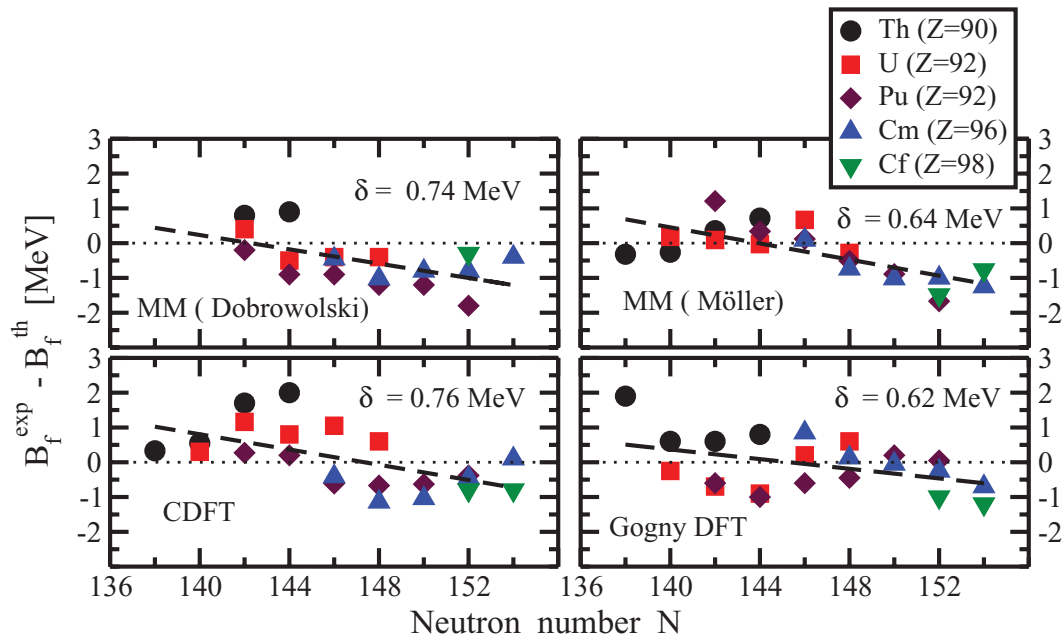

FIG. 2. (Color online) The difference between experimental and calculated heights of inner fission barriers as a function of neutron number N. The results of the calculations are compared to estimated fission barrier heights given in the RIPL-3 database [49], which is used for this purpose in the absolute majority of theoretical studies on fission barriers in actinides. The results of the calculations within the microscopic + macroscopic method (MM(Dobrowolski) [6] and MM(Möller) [7]), covariant density functional theory (CDFT [1]), and density functional theory based on the finite-range Gogny force (Gogny DFT [14]) are shown. Thick dashed lines are used to show the average trend of the deviations between theory and experiment as a function of neutron number. The average deviation per barrier δ (in MeV) is defined as $\delta = \sum_{i=1}^{N} |B_f^i(\text{th}) - B_f^i(\text{exp})|/N$, where N is the number of the barriers with known experimental heights, and $B_f^i(\text{th})$ [$B_f^i(\text{exp})$] are calculated (experimental) heights of the barriers. Long-dashed lines represent the trend of the deviations between theory and experiment as a function of neutron number. They are obtained via linear regression based on a least-squares fit.

TABLE IV. The definition of pairing in the studies of inner fission barriers within the last decade. The first column shows the first author and the reference. The pairing model (BCS or HFB) and type of pairing (G: seniority pairing with fixed strength G, δ: zero-range δ force, and Gogny: finite-range Gogny force) are shown in column 2. Column 3 shows either the region of the nuclear chart or the nucleus in which the fitting of the parameters of the pairing force has been performed in the case of constant G and/or δ pairing. Column 4 shows whether particle number projection (PNP) by means of the Lipkin-Nogami method has been used in the calculations. Column 5 indicates whether the systematic calculations, covering all even-even actinide nuclei with measured inner fission barriers, have been performed (Yes) or not (No). In the case of restricted calculations, the number of nuclei, for which the calculations have been performed is shown. Column 6 is similar to column 5 but for SHE. The calculations are considered to be systematic if they cover a significant range of proton and neutron numbers. The letter "T" ("A") in column 7 indicates that the triaxial deformation is (is not) included in the calculations. Column 8 shows the pairing window used in the calculations with constant G and δ pairing; no pairing window is used in the calculations with the Gogny force. Note that it is not always possible to extract these details from the original publications or references quoted therein. In these cases, the relevant box of the table is empty.

Author [reference] 1	Pairing model 2	Fitting region 3	PNP 4	Actinide 5	SHE 6	A/T 7	E_{cutoff} 8
Macroscopic + microscopic method							
Möller 2009 [7]	BCS(G) [48]		Yes	Yes	Yes	T	
Dobrowolski 2007 [6]	BCS(G)		No	Yes	2	T	
Kowal 2010 [9]	BCS(G)	$Z \geqslant 84$ [51]	No	Yes	Yes	T	
Extended Thomas-Fermi plus Strutinsky integral							
Dutta 2000 [10]	BCS(δ)		No	5	5	T	
Skyrme density functional theory							
Bonneau 2004 [12]	BCS(G)/BCS(δ)	^{254}No/$A \sim 178$	No	Yes	No	A/T[a]	6 MeV
Bürvenich 2004 [52]	BCS(δ)	across nuclear chart [53]	No	Yes	Yes	A	[53][b]
Samyn 2005 [54]	HFB(δ)	$Z \in (92, 98)$[c]	Yes	Yes	Yes	T	different E_{cutoff}[d]
Staszczak 2006 [13]	BCS(G)	^{252}Fm and Ref. [55]	No	Yes	Yes	T	lowest Z (N) states[e]
Staszczak 2007 [56]	BCS(G)/BCS(δ)	^{252}Fm	No	Yes	Yes	T	lowest Z (N) states[e]
Gogny density functional theory							
Warda 2002 [3]	HFB(Gogny)	No	No	5	No	T	No
Delaroche 2006 [14]	HFB(Gogny)	No	No	Yes	No	T	No
Covariant density functional theory							
Bender 1998 [11]	BCS(δ)	across nuclear chart [53]	No	No	3[f]	T	[53][b]
Bürvenich 2004 [52]	BCS(δ)	across nuclear chart [53]	No	Yes	Yes	A	[53][b]
Karatzikos 2010 [57]	RHB(Gogny)[g]	No	No	Yes	Yes	A	No
Abusara 2010 [1]	BCS(G)	$Z \in (90, 100)$ $N - Z \in (42, 66)$	No	Yes	No	T	120 MeV

[a]The calculations with allowance for triaxial deformation have been performed only for four nuclei.

[b]The pairing-active space Ω_q is chosen to include approximately one additional oscillator shell of states above the Fermi level.

[c]The pairing force has been fitted to absolute masses. As a result, it is considerably stronger than the one fitted to even-odd mass differences [54].

[d]The single-particle states in the pairing window $\epsilon_F \pm E_{\text{cutoff}}$ are included. $E_{\text{cutoff}} = 17$ MeV for the BSk6, BSk7, and BSk8 Skyrme forces, $E_{\text{cutoff}} = 15$ MeV for the BSk2 force, $E_{\text{cutoff}} = 16.5$ MeV for the BSk9 force, and $E_{\text{cutoff}} = 5$ MeV for the SLy6 force.

[e]The pairing-active space consisted of the lowest Z (N) proton (neutron) single-particle states.

[f]The calculations with allowance for triaxial deformation have been performed only for a single nucleus.

[g]RHB is the relativistic Hartree-Bogoliubov approach.

on the inner and outer fission barriers. The calculations in this axially symmetric octupole code, abbreviated throughout this paper by (O), vary the function

$$\langle H \rangle + \sum_{\mu=2,3} C_{\mu,0} (\langle \hat{Q}_{\mu,0} \rangle - q_{\mu,0})^2. \quad (19)$$

It was checked that the numerical results obtained for axially symmetric solutions in the A, T, and O calculations differ by no more than 50 keV for all deformations of interest.

The truncation of the basis is performed in all these calculations in such a way that all states belonging to the shells up to $N_F = 20$ fermionic shells and $N_B = 20$ bosonic shells are taken into account. This truncation scheme has been tested and used in the actinides in Ref. [1]. Although the calculations in such a truncation scheme provide sufficient numerical accuracy, they are also very computationally demanding (see Ref. [1] for details). This is the reason why we treat the pairing channel in the present triaxial RMF calculations in the BCS approximation despite the fact that the triaxial cranked relativistic Hartree + Bogoliubov (RHB) approach
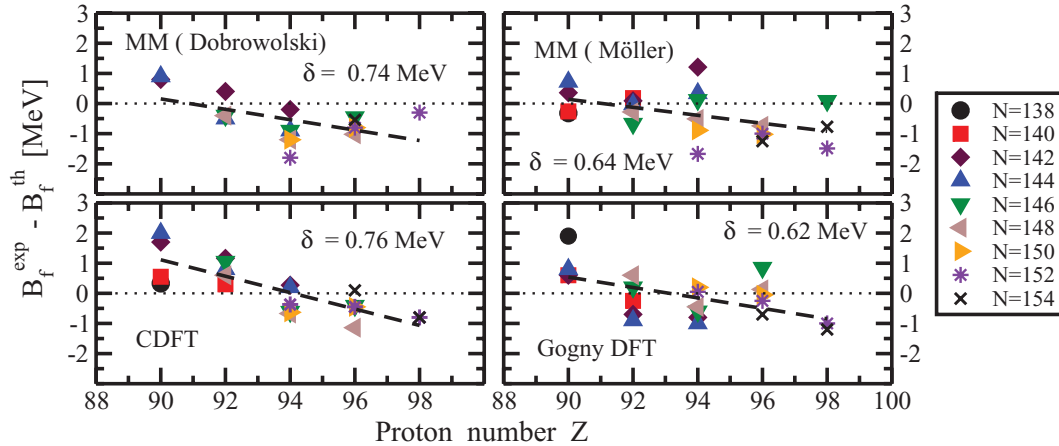
FIG. 3. (Color online) The same as in Fig. 2 but as a function of proton number Z.

with finite-range Gogny forces in the pairing channel was developed in the late 1990s [61,62]. RMF + BCS calculations are less time consuming and more stable (especially, in the saddle-point region) than the RHB calculations.

Figure 1 shows an example of the distribution of deformation points on a PES at which the numerical results were obtained using these constraints in a triaxial (T) calculation.

All mean-field calculations for fission barriers with triaxiality included are computationally demanding. This is the reason why simple pairing interactions (either seniority pairing with constant strength G or the zero-range δ-force) and the BCS framework are used in the majority of the calculations (see Table IV). The overview given in this table focuses mainly on the investigations including triaxial deformation and on the most recent and comprehensive studies within the specific theoretical frameworks. In particular, the studies of fission barriers in superheavy elements (SHE) are included irrespective of whether or not the calculations include triaxial deformation. This table shows that the majority of studies neglect particle number projection and use different prescriptions for the size of the pairing window. The impact of these prescriptions on the height of the inner fission barrier has recently been investigated in Ref. [57].

The inclusion of triaxiality has improved the accuracy of the description of the inner fission barriers in actinides in all state-of-the-art models [1,6,7,14]. Figures 2 and 3 show the differences between experimental and calculated heights of inner fission barriers obtained in different theoretical models as a function of neutron and proton numbers, respectively. Note that this comparison covers only results of systematic triaxial calculations which simultaneously include even-even Th, U, Pu, Cm, and Cf nuclei. To our knowledge, no such calculations have been published with DFT based on Skyrme forces. As a result, these figures cover all existing systematic triaxial studies of inner fission barriers in actinides.

The δ values displayed on the panels of Figs. 2 and 3 show the average deviation from experiment for the calculated heights of inner fission barriers. One can see that they are of the same magnitude in the different approaches and minor differences between the approaches in the δ values are not

important given the considerable uncertainties in the extraction of inner fission barrier heights from experimental data as seen, for example, in the differences of the compilations of Refs. [49,65].

However, the similarity of the average trends of these deviations (shown by thick dashed lines in Figs. 2 and 3) as a function of neutron and proton numbers is more important given the differences in the underlying mean fields and in the treatment of pairing correlations. At present, it is difficult to find a clear explanation for these trends. Although differences in the treatment of pairing correlations (BCS with monopole pairing and of different pairing windows in the CDFT [1] and MM [6,7] calculations versus the Hartree-Fock-Bogoliubov framework based on the D1S force in Gogny DFT [14]) can contribute to deviations between theory and experiment [57], it is quite unlikely that they are responsible for the observed trends of the deviations.

III. RESULTS AND DISCUSSION

The nucleus $^{292}120$ is predicted to be a spherical doubly magic nucleus in CDFT [11,66]. Its potential energy surface in the β-γ plane is shown in Fig. 4. It is interesting to compare it with the PES of the nucleus ^{240}Pu shown in Fig. 1. These two potential energy surfaces are representative examples of typical potential energy surfaces in actinides and superheavy nuclei. The gross structure of these two is defined by the fact that the total energy is generally increasing when moving away from the $\gamma = 0°$ axis—so it looks like a canyon. However, there are local structures inside the canyon which define the differences between the two mass regions with respect to the impact of triaxiality on the inner and outer fission barriers.

In ^{240}Pu, a large hill is located at the axial shape $\beta_2 \sim 0.5$ inside a canyon. As a consequence, the fission path from the normal deformed minimum initially proceeds along the $\gamma = 0°$ axis, then bypasses the axial $\beta_2 = 0.5$ hill via a path with $\gamma \sim 10°$, and then proceeds along the bottom of the canyon on an axially symmetric path again. As a result of this bypass, the inner fission barrier heights of the actinides are lowered by
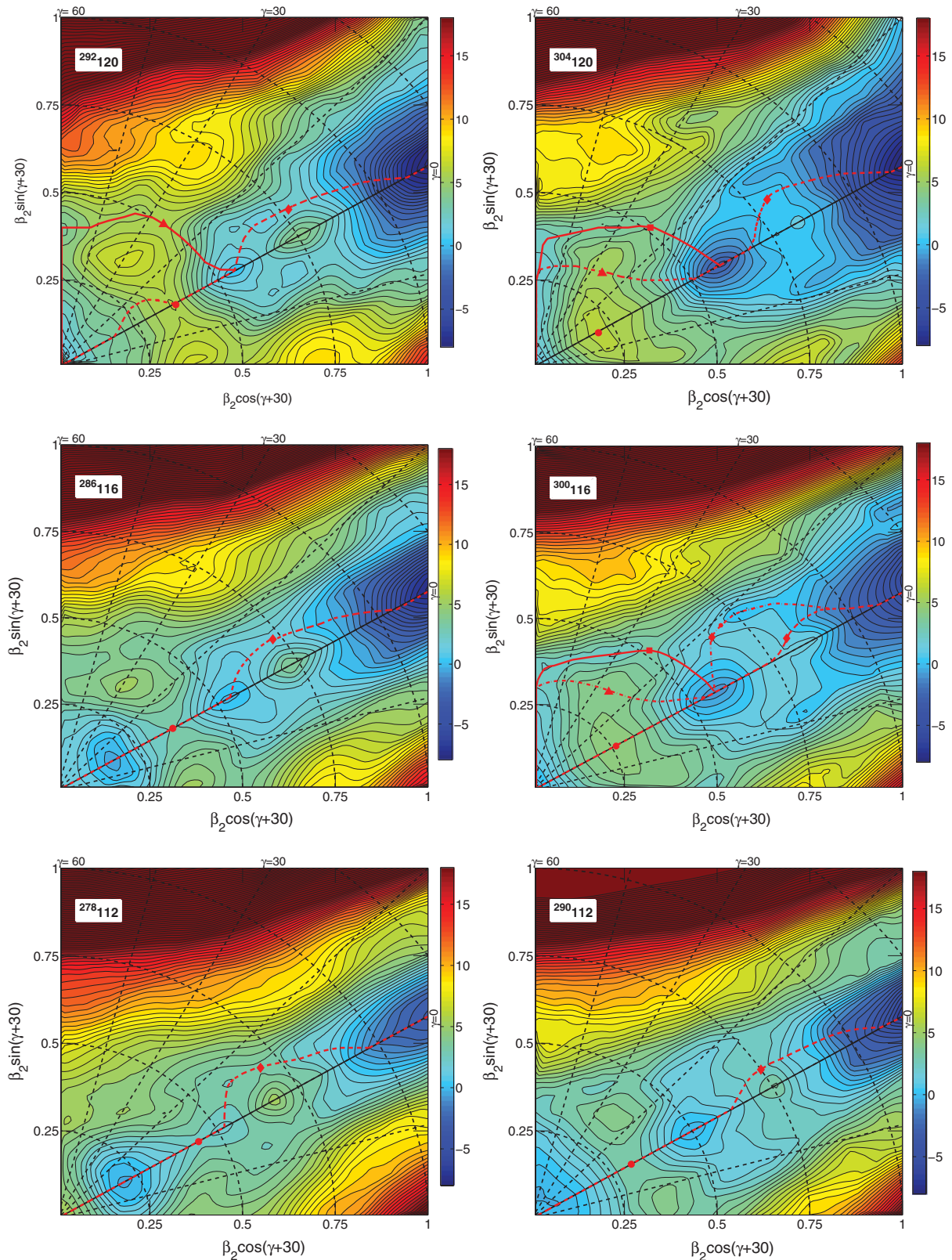
FIG. 4. (Color online) Potential energy surfaces of selected nuclei. The energy difference between two neighboring equipotential lines is equal to 0.5 MeV. The saddles along the Ax, Tr-A, and Tr-B fission paths are shown by solid circles, triangles, and squares, respectively. The solid diamonds show the outer fission barrier saddles. The saddles are defined via the immersion method [7], while the fission paths are defined as minimum energy paths [63,64] which represent the most probable pathway connecting two minima via a given saddle. Note that in contrast to other nuclei there are two possible fission paths for the outer fission barrier in the ^{300}116 nucleus.

$1-4$ MeV due to triaxiality [1]. However, the calculated outer fission barriers of the actinides are not affected by triaxiality [1].

The properties of the PES of the nucleus $^{292}120$, defining the fission paths, are completely opposite to the case of ^{240}Pu since there are two triaxial hills and one axial one inside the PES canyon of $^{292}120$. The two triaxial hills are located at moderate deformations ($\beta_2 \sim 0.35$, $\gamma \sim \pm 30°$), while the axial hill is superdeformed ($\beta_2 \sim 0.75$). The fission path (shown by a red dashed line in Fig. 4) starts at a spherical shape, then proceeds between two triaxial hills ($\beta_2 \sim 0.35$, $\gamma \sim 30°$), and bypasses the axial hill at $\beta_2 \sim 0.75$ via a $\gamma \sim 7°$ path. The γ-softness of the PES, which exists between the two triaxial hills, has only a minor effect on the height of the inner fission barrier; the triaxial solution is lower than the axial one by 100–200 keV at $\beta_2 = 0.2$–0.3 deformations (see Fig. 5). However, this figure shows that *along this fission path* the height of the inner fission barrier is not affected by triaxiality.

The second fission path shown by a solid red line starts at a spherical shape and proceeds along the axially symmetric $\gamma = 60°$ axis, via a saddle point at ($\beta_2 \sim 0.47$, $\gamma \sim 21°$) and then along the first fission path after second minimum. The existence of the valley between the walls of the canyon and triaxial hills at ($\beta_2 \sim 0.35$, $\gamma \sim \pm 30°$) is a necessary condition for the existence of this path. This type of fission path exists in a number of nuclei, so for convenience we will call it a triaxial Tr-B fission path. The unusual physical feature of this second path is the fact that initially the nucleus has to be squeezed along the axis of symmetry, thus creating an
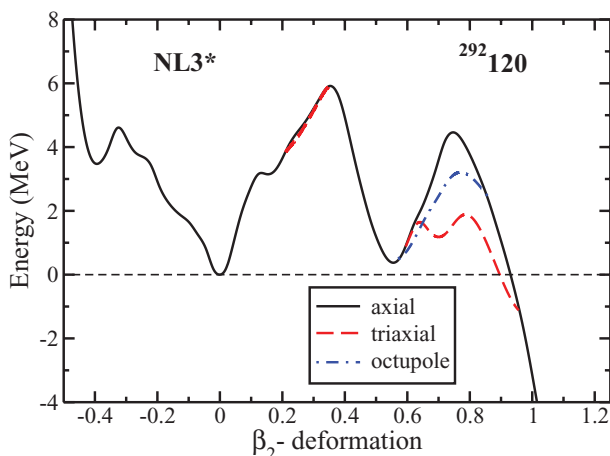

FIG. 5. (Color online) Deformation energy curves for the $Z = 120$, $N = 172$ nucleus obtained with the NL3* parametrization. The black solid, red dashed, and blue dot-dashed lines display the deformation energy curves for the axially symmetric, triaxial, and axial octupole deformed solutions. We show the deformation energy curves for the last two solutions only in the range of β_2 values where it is lower in energy than the deformation energy curve of the axially symmetric solution. Note that the Tr-B fission path via the saddle at $\beta_2 = 0.47$, $\gamma = 26°$ (see text for details) is not shown since this saddle is lower than the one of the Ax fission path only by 0.2 MeV (see Table V); the results of Ref. [67] suggest that spontaneous fission exploiting this path is less likely than the one along the Ax fission path.

oblate nucleus with quadrupole deformation $\beta_2 \sim -0.39$. This is contrary to the usual picture of fission where the prolate or near-prolate nucleus is stretched out along the path of increasing quadrupole deformation. Note that the saddle of this fission path is only by 0.2 MeV lower than the saddle of the first fission path (see Table V) and in addition it is much longer. Therefore, by considering a dynamical calculation taking into account the action integral along the entire fission path [67] this path will probably not contribute much to the fission probability.

Contrary to the actinides, the triaxiality has a considerable impact on the shape and the height of the outer fission barrier, which is lowered by ~ 3 MeV in the $^{292}120$ nucleus (see Fig. 5). Note that, in this nucleus, the lowering of the outer fission barrier due to octupole deformation is substantially smaller than the one due to triaxiality.

It is also evident that the landscape of the PES and the existence of saddle points and valleys depends on the proton and neutron numbers. This is clearly seen in Fig. 4 and in Table V. In the $Z = 120$ isotopes, the increase of neutron number up to $N = 184$ and beyond leads to the emergence of an axial hill at $\beta_2 \sim 0.2$–25; this is clearly visible in the nucleus $^{304}120$ in Fig. 4. Its existence in high-Z and neutron-rich nuclei leads to the shift of the first fission path in the deformation space. In lighter systems this path proceeds via the axially symmetric saddle as, for instance, in the nucleus $^{292}120$ in Fig. 4. For heavier systems it starts at spherical shape,[1] proceeds along the axially symmetric $\gamma = 60°$ axis up to $\beta_2 \sim 0.25$, and then via a saddle point at ($\beta_2 \sim 0.32$, $\gamma \sim 26°$), located between a triaxial ($\beta_2 \sim 0.35$, $\gamma \sim 28°$)[2] and an axial $\beta_2 \sim 0.2$ hill, to the axially symmetric superdeformed minimum. This type of fission path exists in a number of nuclei. We will label it as triaxial Tr-A for convenience. In addition, there is a second triaxial path Tr-B via a saddle at $\beta_2 \sim 0.5$, $\gamma \sim 22°$, which is similar to the one present in the nucleus $^{292}120$.

The structure of the PES of the nucleus $^{300}116$ is similar to the one of the nucleus $^{304}120$ in Fig. 4. The lowering of neutron number below $N = 184$ in the nuclei under study leads to the situation that the fission path via the axially symmetric inner saddle (called Ax below) becomes energetically favored. This is clearly seen in the PES of the $^{286}116$, $^{278}112$, and $^{290}112$ nuclei in Fig. 4 and in Table V.

It is clear that the landscape of the PES of superheavy nuclei in the region of the inner fission barrier is more complicated than in the case of the actinides. The energetically favored fission path in the majority of these nuclei proceeds through an axially symmetric saddle (see Fig. 4 and Table V). Only in a few nuclei ($^{304,306,308}120$, $^{300,302,304}118$, and $^{300}116$) is

---

[1]As discussed later, some of the nuclei have superdeformed ground states. However, the calculated outer fission barriers are rather small (~ 2 MeV relative to the superdeformed minimum), which suggests that these states are extremely unstable against fission. Thus, we start the discussion from spherical or weakly (normal) deformed minima which have better survival probability against fission.

[2]This hill is clearly visible when the energy difference between two neighboring equipotential lines is set to 0.1 MeV (see Fig. 12 below).
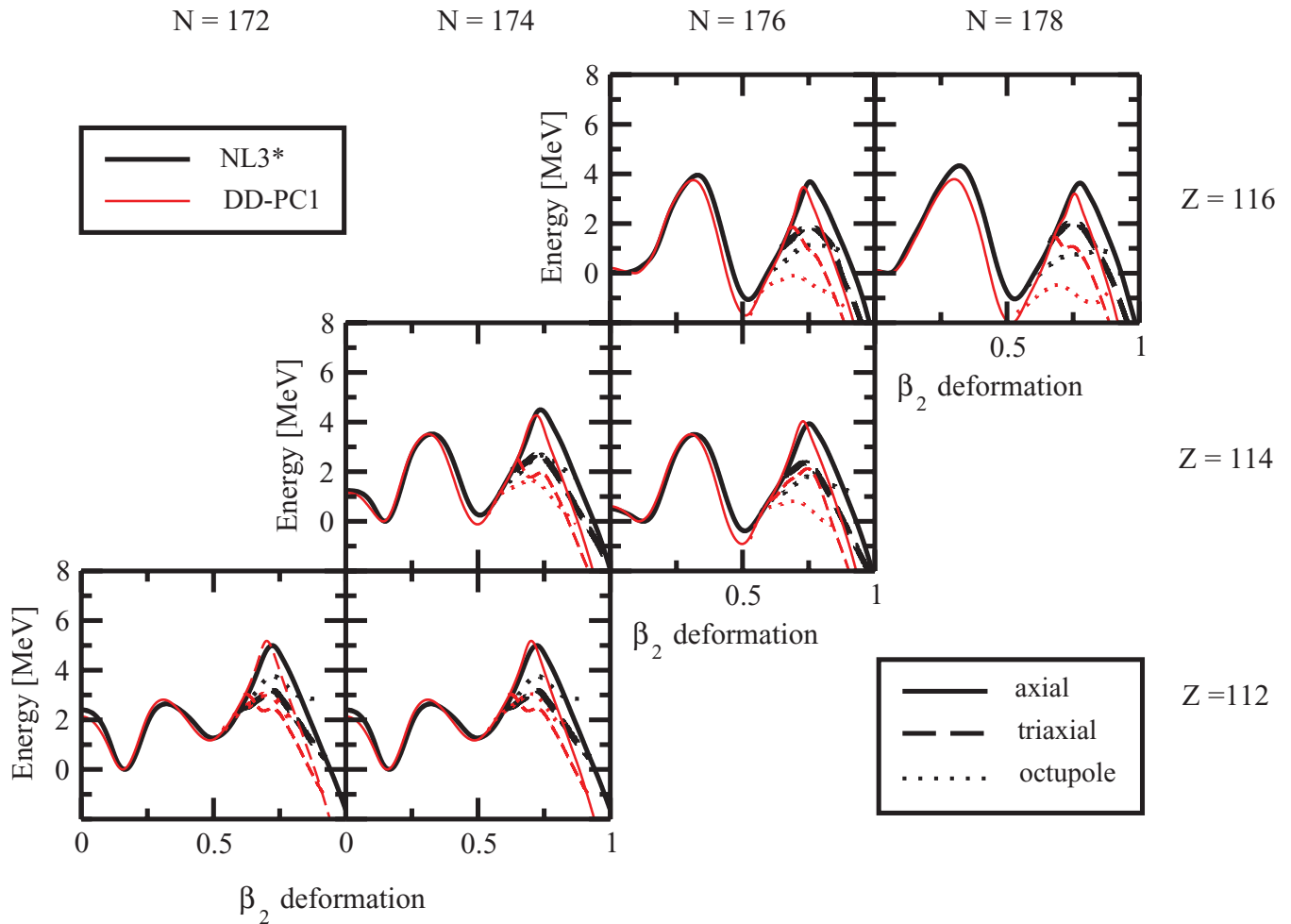
FIG. 6. (Color online) Deformation energy curves for the $Z = 112$, 114, and 116 nuclei obtained with the NL3* and DD-PC1 parametrizations of the RMF Lagrangian. Solid lines correspond to axial solutions with reflection symmetry (A), dashed lines to triaxial solutions with reflection symmetry (T), and dotted lines to octupole deformed solutions with axial symmetry (O). Note that the T and O solutions are shown only in the deformation range in which they are lower in energy than the axial solution.

the triaxial fission path Tr-A lower in energy than the axial Ax fission path. The triaxial fission path Tr-B exists in the majority of the nuclei apart from neutron-poor $Z = 114$ nuclei and $Z = 112$ nuclei (see Fig. 4 and Table V). The energy of the saddle point of this fission path is lower than the one of the first fission path (either Ax or Tr-A) in a number of nuclei. However, the results of calculations within the MM method [67] suggest that, although triaxiality lowers the static fission barriers, it plays a minor role in spontaneous fission of superheavy nuclei with $Z \leqslant 120$. This is because a fission path via an oblate shape and triaxial saddles is substantially longer compared to the axially symmetric path, which leads to a significant reduction of the penetration probability. However, this complexity of the PES and the presence of two fission paths for the inner fission barriers calls for finding the dynamical path along which the fission process takes place in CDFT. Work in this direction is in progress.

Figures 6 and 7 show deformation energy curves for several isotopes with charge numbers $Z = 112$, 114, and 116 for three classes of CDFT models. Experimental estimates of the

inner fission barrier heights were obtained for these nuclei in Ref. [68]. The potential energy structure of these nuclei is similar to the one seen in $^{292}120$ (Fig. 4); the presence of two triaxial hills at moderate deformations ($\beta_2 \sim 0.35$, $\gamma \sim \pm 30°$) defines two possible fission paths: one between the hills (either Ax or Ax-Tr paths) and another between the hill and the walls of the PES canyon (Tr-B path). The γ-softness of the PES, which exists between the two triaxial hills, defines whether the fission path passing between these two hills is fully axially symmetric (Ax path) or has some degree of triaxiality (Ax-Tr path). The Ax-Tr path is generally similar to the Ax path but differs from it by the fact that moderate triaxiality ($\gamma \leqslant 10°$) appears at the saddle and along the shoulder of the inner fission barrier. Although the heights of the discussed hills in the region of inner fission barrier depends on the parametrization, the observed features of the potential energy surfaces and fission paths are rather independent of the parametrization (Fig. 8). Tables V, VI and VII show that the saddle point along this path has triaxiality only in the case of the two nuclei $^{292,294}114$. However, even in these cases the Ax
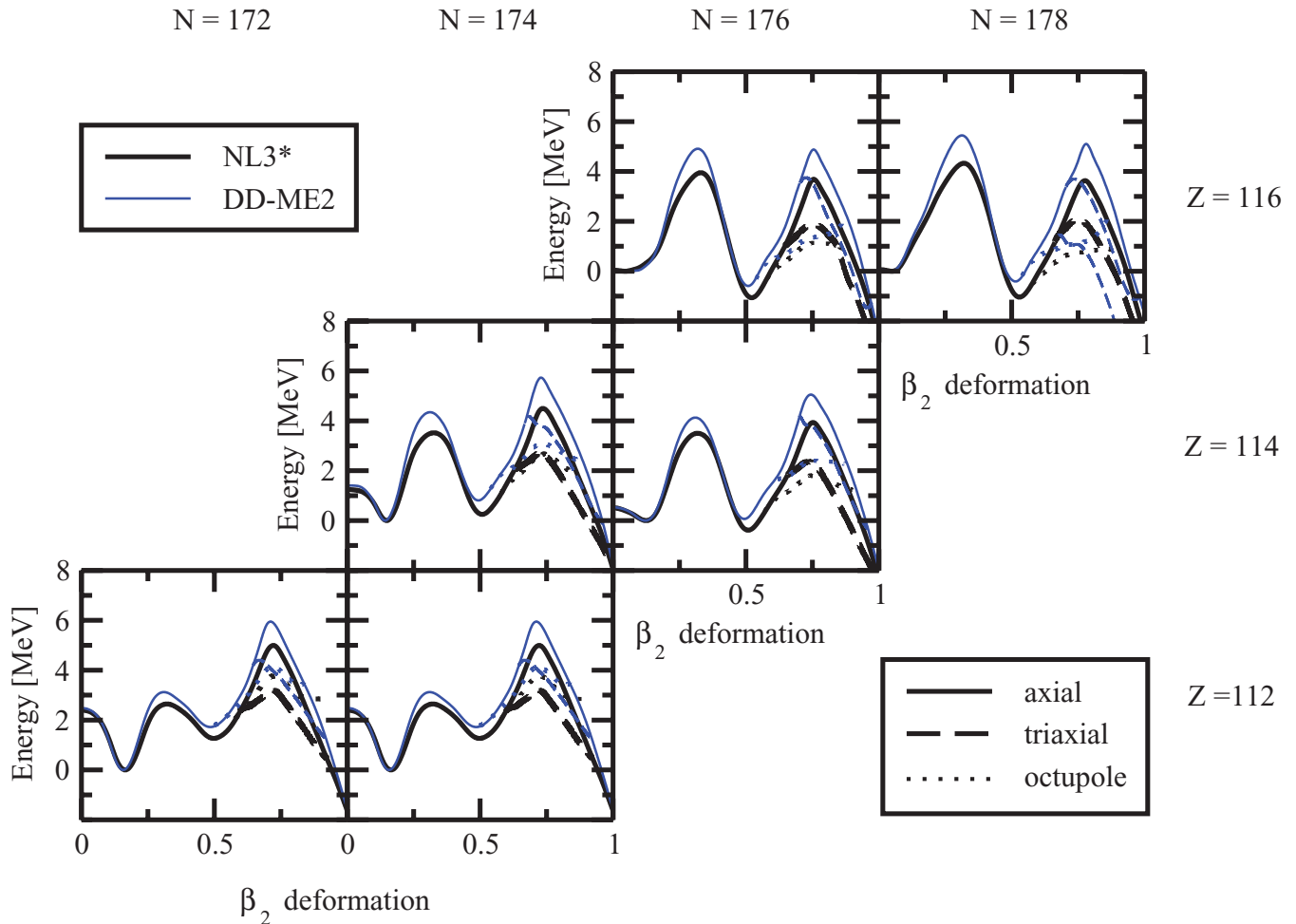
FIG. 7. (Color online) The same as Fig. 6 but for the NL3* and DD-ME2 parametrizations.

saddle is only 50–150 keV higher than the Tr-A saddle. Thus, similarly to the ^{292}120 nucleus, triaxiality only marginally affects the inner fission barriers. Note that the ground states are somewhat deformed in these nuclei [see Figs. 6 and 9(a)].

For these nuclei triaxiality has a considerable impact on the shape and height of the outer fission barriers; the decrease of the heights of the outer fission barriers due to triaxiality is typically in the range of 1.5–2.0 MeV and it depends on the particle number and on the RMF parametrization. Note that the outer fission barriers are affected also by octupole deformation. In the $Z = 112$ nuclei, the triaxial saddle is lower in energy than the octupole saddle. The situation is reversed in the $Z = 114, 116$ nuclei.

Among the different classes of CDFT models, the DD-ME2 parametrization always gives the highest values for the inner and outer fission barrier heights. They are (on average) by 1 and 1.5 MeV higher than the ones obtained in the NL3* and the DD-PC1 parametrizations. The heights and the shapes of the inner fission barriers are very similar for the NL3* and DD-PC1 parametrizations. The outer fission barriers also come close to each other in these two parametrizations in axial [A], triaxial [T], and octupole [O] (for $Z = 112$ nuclei) calculations. However, with Z increasing from 114 to 116 the difference between the results of octupole calculations

increases; the difference between the energies of the octupole saddles obtained in the NL3* and DD-PC1 parametrizations reaches 2 MeV in the $Z = 116$ nuclei (see Fig. 6).

There is only one experimental work [68] where estimates on the heights of inner fission barriers in superheavy nuclei with $Z = 112, 114$, and 116 have been obtained. Unfortunately, experimentally the fission barriers are accessible only indirectly and a model-dependent analysis is used to obtain these quantities, which causes an ambiguity in the comparison with theoretical results. Even in the actinide region where the fission barrier heights were extracted from a number of independent experiments with high statistics (see, for example, Ref. [7]), a typical uncertainty in the experimental values, as suggested by the differences among various compilations, is of the order of ± 0.5 MeV [54]. These uncertainties are expected to be higher in superheavy nuclei since the estimates of Ref. [68] are based on experimental data represented by low statistics and on a method which differs from the methods used in the analysis of fission barrier heights in actinides. In addition, there is no independent confirmation of the inner fission barrier height estimates of Ref. [68]. The interpretation of experimental data based on cross sections in terms of fission barrier heights becomes even more complicated when the fission path has a double-hump structure, which according to many calculations
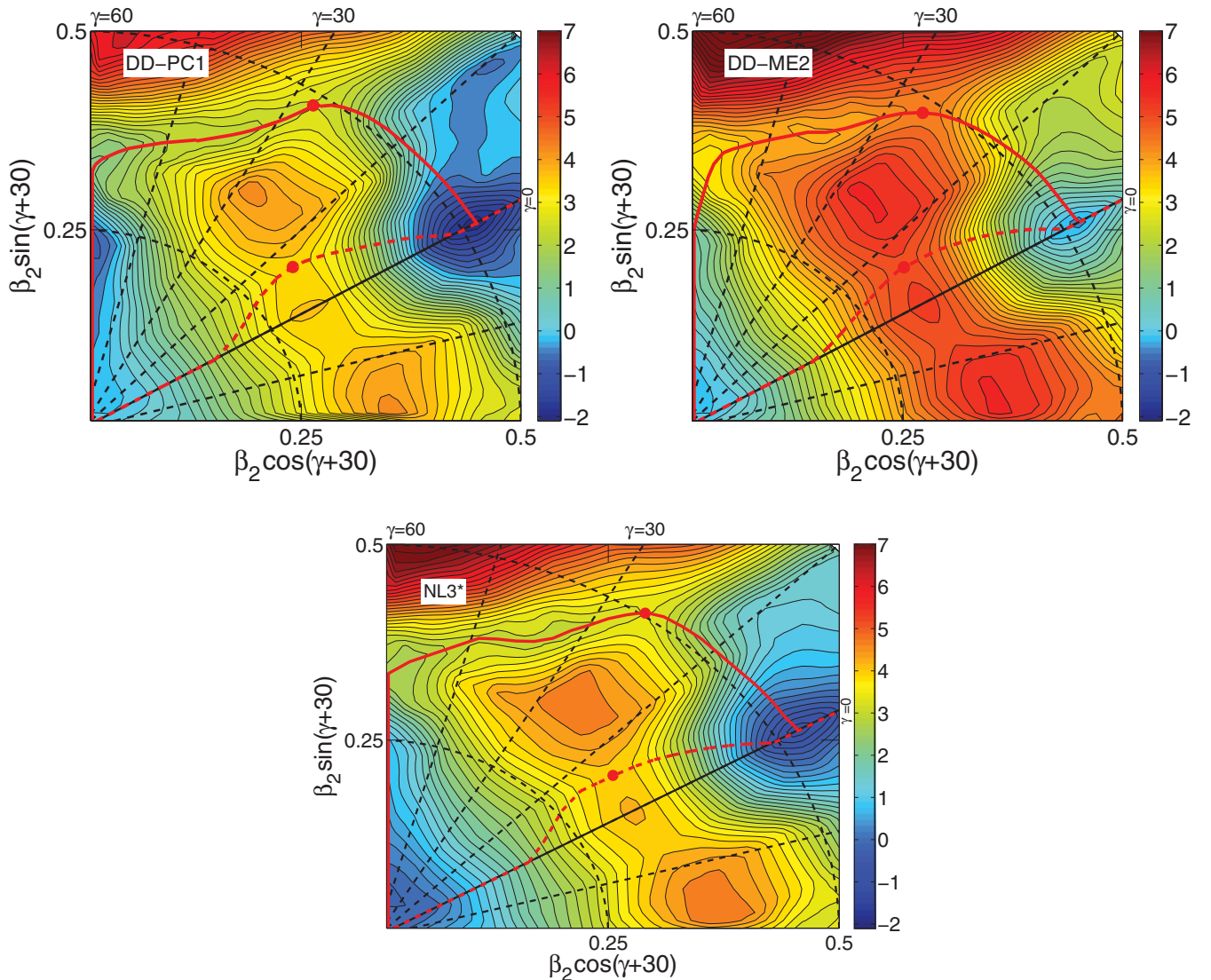
FIG. 8. (Color online) The same as in Fig. 4 but for the nucleus ^{294}116. The results are shown for the parametrizations NL3*, DD-PC1, and DD-ME2. The energy difference between two neighboring equipotential lines is equal to 0.2 MeV.

may be the case in superheavy nuclei. The widening of the barrier due to the second hump (or its remnant) would require the lowering of the inner fission barrier height; this possibility has not been taken into account in the analysis of Ref. [68]. Based on this discussion it is clear that the level of confidence of fission barrier height estimates for superheavy nuclei is significantly lower than the one for the actinides.

According to Ref. [68], the estimated lower limits for fission barrier heights in even-even $Z = 112, 114,$ and 116 nuclei shown in Figs. 6 and 7 are 5.5, 6.7, and 6.4 MeV, respectively. Our results for the heights of the inner fission barrier in these nuclei along the Ax and Ax-Tr fission paths are always smaller than the experimental data by 1–3 MeV. The saddle along the Tr-B fission path is somewhat lower in energy (by 0.4–0.7 MeV) than the saddle along the Ax-Tr path in ^{292,294}116 nuclei (see Table VII). However, as discussed above (based on the results of Ref. [67]) it is unlikely that the fission predominantly proceeds along the Tr-B path

considering especially (i) that the gain in saddle-point energy compared with the Ax-Tr path is small and (ii) the Tr-B path is substantially longer compared with the Ax-Tr path.

Given the discussion above, it is not clear at this moment how serious the discrepancy between calculations and experimental estimates is. However, the results of the calculations suggest one possible way to increase the heights of inner fission barriers. Potential energy surfaces in the ground-state region of these nuclei are extremely soft (see Figs. 6 and 7). For such nuclei, the correlations beyond mean field (taken into account, for example, by the generator coordinate method) can lower the energy of the ground state by a few MeV without affecting much the barrier top, thus effectively increasing the height of the inner fission barrier.

Systematic calculations of inner fission barriers have been performed for even-even $Z = 112$–120 nuclei with $N - Z = 52$–68 using the NL3* parametrization. This is the same parametrization which has been used in systematic

TABLE V. The heights of axially symmetric (Ax) and triaxial (Ax-Tr, Tr-A, and Tr-B) saddle points (in MeV) with respect to spherical or weakly (normal) deformed minima and their deformations. Note that only the quadrupole deformation is given for the axial saddle. Columns 4 and 5 show the values for the saddles of either Ax-Tr or Tr-A fission paths. The asterisk to the fission barrier height in column 4 indicates that the values for the Ax-Tr path are displayed; the absence of the asterisk implies that the values for the Tr-A path are shown. Note that triaxial saddles are shown only in the cases when their heights are lower than those of the axial saddle.

Nucleus 1	B_f^{Ax} 2	β_2 3	B_f^X 4	(β_2,γ) 5	B_f^{Tr-B} 6	(β_2,γ) 7
			$Z = 120$ nuclei			
^{308}120	5.11	0.20	3.04	(0.34,26°)	2.23	(0.48,22°)
^{306}120	5.00	0.20	3.46	(0.33,26°)	2.02	(0.50,22°)
^{304}120	5.46	0.21	4.51	(0.33,26°)	3.30	(0.51,21°)
^{302}120	5.37	0.19	5.00	(0.33,25°)	3.93	(0.50,24°)
^{300}120	5.35	0.32	4.93∗	(0.31,11°)	4.08	(0.50,26°)
^{298}120	5.35	0.33	5.02∗	(0.33,12°)	4.27	(0.49,28°)
^{296}120	5.67	0.34	5.57∗	(0.35,10°)	4.92	(0.50,27°)
^{294}120	5.27	0.34			4.73	(0.50,27°)
^{292}120	5.82	0.36			5.61	(0.50,27°)
			$Z = 118$ nuclei			
^{304}118	4.97	0.21	3.92	(0.33,26°)	3.03	(0.51,26°)
^{302}118	5.07	0.23	4.57	(0.33,26°)	3.41	(0.51,25°)
^{300}118	5.18	0.28	4.94∗	(0.27,15°)	3.37	(0.51,26°)
^{298}118	5.07	0.32	4.72∗	(0.32,12°)	3.67	(0.50,27°)
^{296}118	5.00	0.32	4.73∗	(0.33,10°)	3.87	(0.50,26°)
^{294}118	4.95	0.32	4.82∗	(0.33,10°)	4.12	(0.50,25°)
^{292}118	4.75	0.34			4.35	(0.50,23°)
^{290}118	4.15	0.36			4.08	(0.49,24°)
^{288}118	3.28	0.36				
			$Z = 116$ nuclei			
^{300}116	4.83	0.26	4.48	(0.35,25°)	3.13	(0.52,22°)
^{298}116	4.78	0.28	4.57	(0.30,15°)	3.29	(0.51,23°)
^{296}116	4.53	0.32	4.32∗	(0.32,11°)	3.35	(0.51,24°)
^{294}116	4.37	0.32	4.22∗	(0.33,7°)	3.40	(0.50,25°)
^{292}116	3.98	0.33	3.93∗	(0.34,7°)	3.39	(0.48,26°)
^{290}116	3.39	0.34			3.47	(0.48,27°)
^{288}116	3.55	0.34				
^{286}116	3.43	0.36				
^{284}116	3.40	0.37				
			$Z = 114$ nuclei			
^{296}114	4.65	0.28	4.43∗	(0.31,15°)	3.42	(0.49,24°)
^{294}114	4.19	0.29	4.14∗	(0.31,10°)	3.08	(0.49,25°)
^{292}114	3.81	0.32			3.18	(0.48,25°)
^{290}114	3.40	0.34			3.38	(0.48,26°)
^{288}114	3.52	0.32				
^{286}114	3.32	0.33				
^{284}114	3.07	0.38				
^{282}114	3.08	0.42				
^{280}114	3.20	0.42				

calculations of fission barriers in actinides [1] and which provides 0.76 MeV average deviation from experiment for the heights of inner fission barriers in these nuclei. For a given proton number Z a sequence of nine even-even nuclei is selected such that the middle nucleus of this sequence

roughly corresponds to an experimentally observed nucleus (or a nucleus which is expected to be observed in the near future). This crudely outlines the region which may be experimentally studied within the next one or two decades. The results of these calculations are summarized in Table V and VI.

Based on the results of Ref. [67], it is reasonable to neglect the path Tr-B since it is substantially longer compared with other paths, which leads to significant reduction of the penetration probability. In Fig. 9(b) we consider the evolution of the heights of the inner fission barriers as a function of the neutron number N. The $Z = 112$, 114, and 116 isotope chains show a generally increasing trend for the barrier heights with increasing neutron number for $N \geqslant 172$. Figure 9(a) suggests that the origin of this trend can be traced back to the deformation of the ground state. For small neutron numbers these nuclei are deformed in the ground state. However, they gradually become spherical when approaching $N = 184$ because there is a spherical shell gap at this neutron number (see, for example, Fig. 28 in Ref. [66]). The negative shell correction energy at the ground state is larger in absolute value in the vicinity of the $N = 184$ spherical shell gap than at lower neutron numbers, where the ground state is deformed and characterized by a larger level density in the vicinity of the Fermi level. The level density (and, as a consequence, the shell correction energy) at the saddle point of the inner fission barrier does not change so drastically as the one at the ground state. As a result, the heights of inner fission barriers, which are defined as the energy differences between the binding energies of the ground state and saddle point, show the observed features. Note that in these nuclei the energies of the Ax and Ax-Tr saddles differ by at most 200 keV; the difference between the energies of the Ax and Tr-A saddles does not exceed 400 keV.

The nuclei with $Z = 118$ and 120 have, with the exception of the nucleus ^{288}118, spherical minima due to the presence of the $Z = 120$ spherical shell gap. The nucleus ^{292}120 has the highest value for the fission barrier among all nuclei under investigation. This is connected with its doubly magic nature in CDFT. In the isotope chain with $Z = 120$, moving away from the $N = 172$ shell closure, shell effects connected with spherical shape become less pronounced and this leads to a decrease of the inner fission barrier, because the barrier height in these nuclei is defined with respect to the spherical ground state. Apart from the lightest two and the heaviest $Z = 118$

TABLE VI. The same as Table V but for $Z = 112$ nuclei.

Nucleus 1	B_f^{Ax} 2	β_2 3	B_f^X 4	(β_2,γ) 5	B_f^{Tr-B} 6	(β_2,γ) 7
			$Z = 112$ nuclei			
^{292}112	3.94	0.30			3.64	(0.48,27°)
^{290}112	3.48	0.31			3.44	(0.47,26°)
^{288}112	3.07	0.31				
^{286}112	2.90	0.32				
^{284}112	2.65	0.32				
^{282}112	2.35	0.41				
^{280}112	2.70	0.43				
^{278}112	3.06	0.44				
^{276}112	3.34	0.44				

TABLE VII. The same as in Table V but only for nuclei where experimental estimates of inner fission barrier heights exist. The results of calculations with the DD-PC1 and DD-ME2 parametrizations are presented.

Nucleus	B_f^{Ax}	β_2	B_f^{X}	(β_2,γ)	$B_f^{\text{Tr-}B}$	(β_2,γ)
DD-PC1 parametrization						
^{294}116	3.64	0.31	3.47*	(0.32,10°)	2.58	(0.48,27°)
^{292}116	3.63	0.32	3.55*	(0.32,5°)	2.83	(0.49,26°)
^{290}114	3.42	0.34				
^{288}114	3.38	0.32				
^{286}112	3.02	0.31				
^{284}112	2.75	0.31				
DD-ME2 parametrization						
^{294}116	5.36	0.32	5.20*	(0.32,8°)	4.45	(0.48,25°)
^{292}116	4.77	0.32	4.68*	(0.32,5°)	4.24	(0.48,27°)
^{290}114	4.33	0.34				
^{288}114	4.18	0.32				
^{286}112	3.62	0.31				
^{284}112	3.12	0.31				

isotopes, the fission barrier heights of the $Z = 118$ chain are nearly constant as a function of neutron number and they are close to 4.5 MeV. Note that in these nuclei the energies of the Ax and Ax-Tr saddles differ only by $100-400$ keV. However, the difference between the energies of the Ax and Tr-A saddles can reach 2 MeV (as in the case of the nucleus ^{308}120; see Table V).

It is important to mention that the valley between the axial $\beta_2 \sim 0.2$ and triaxial $\beta_2 \sim 0.40$, $\gamma \sim 25°$ hills leading to a Tr-A saddle is rather shallow. Its depth with respect to the tip of the triaxial hill varies between 100 and 300 keV. The latter value is obtained, for example, in the ^{302}120 nucleus (see Fig. 12 below).

It is interesting to compare the current results with the ones obtained in other models. The results of Skyrme DFT calculations of Ref. [13] for the $N = 184$ isotones show that the impact of triaxiality on the inner fission barrier is small for $Z = 112$, but it increases with increasing Z (see Fig. 4 in Ref. [13]). The lowering of the inner fission barrier due to triaxiality is around 2 MeV for $Z = 120$ and exceeds 3 MeV for $Z = 126$. In the ETFSI model calculations [10] the inner fission barriers are lowered due to triaxiality in the nuclei ($Z = 112$, $N = 182$) and ($Z = 114$, $N = 184$) by 0.5 and 1.1 MeV, respectively. In the macroscopic + microscopic calculations of Ref. [9] the largest reduction of the inner barrier height due to triaxiality is about 2 MeV and it appears in the region around $Z \approx 122$, $N \approx 180$ (see Fig. 2 in Ref. [9]).

As discussed in Ref. [1] on the example of actinide nuclei, the reduction of the inner fission barrier height due to triaxiality is caused by the level densities in the vicinity of the Fermi level, which are lower at triaxial shape than at axial shape. The different locations of the "magic" shell gaps in superheavy nuclei in the macroscopic + microscopic model (at $Z = 114$, $N = 184$), in Skyrme DFT (predominantly at $Z = 126$, $N = 184$), and in CDFT (at $Z = 120$, $N = 172$) result in different deformed single-particle structures at the deformations typical for the saddles of the inner fission barrier.
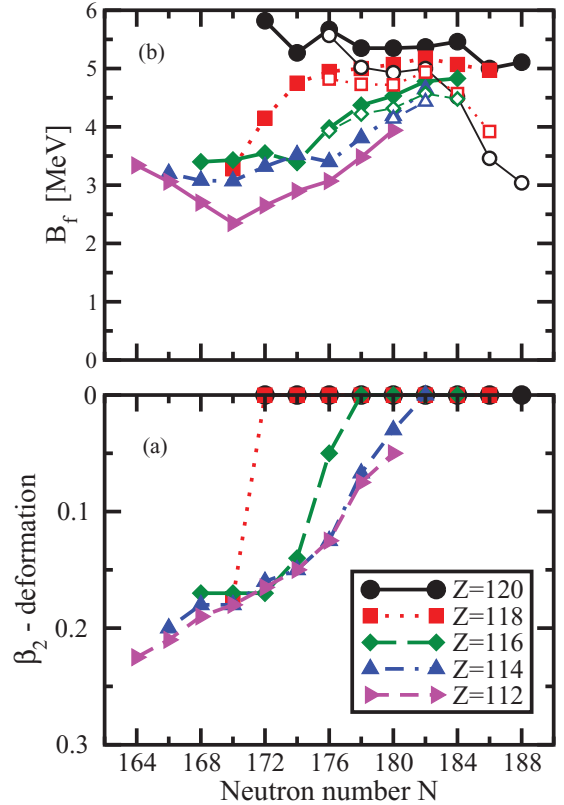

FIG. 9. (Color online) (a) The deformations of the ground states of even-even $Z = 112$–120 nuclei as a function of neutron number. (b) The energies of axial (large solid symbols, thick lines) and triaxial (either Ax-Tr or Tr-A; shown by small open symbols and thin lines) saddles with respect to the spherical or weakly (normal) deformed minima in these nuclei as a function of neutron number. Note that the same type of symbols is used for axial and triaxial saddles in a given isotope chain.

This is one of the sources of the differences in the predictions of different models.

We have to keep in mind, however, that we use in this investigation a seniority-zero pairing force with a fixed cutoff energy of $E_{\text{cutoff}} = 120$ MeV. It has been shown in Ref. [57] that pairing correlations play an important role for the calculation of the fission barriers and that even if the strength of the pairing force is adjusted to experimental gap parameters at the ground state, the range of the pairing force has an influence on the height of the barrier. This means that for zero-range forces and for the seniority-zero forces the barriers depend on the cutoff energy. It also has been shown in Ref. [57] that the parameter set DD-ME2 in connection with the finite-range Gogny force D1S in the pairing channel produces in axial symmetric calculations in most of the actinide nuclei inner barriers which are too high as compared with experiment (see Fig. 9 of Ref. [57]) and that it produces for the superheavy elements with $Z = 112$, 114, and 116, where experimental estimates are available [68] in axially symmetric calculations barriers which are in rather good agreement with those values (see Fig. 10 of Ref. [57]). Of course, so far, there exist no relativistic triaxial calculations with the finite-range Gogny force in the pairing channel and full Gogny calculations [14]
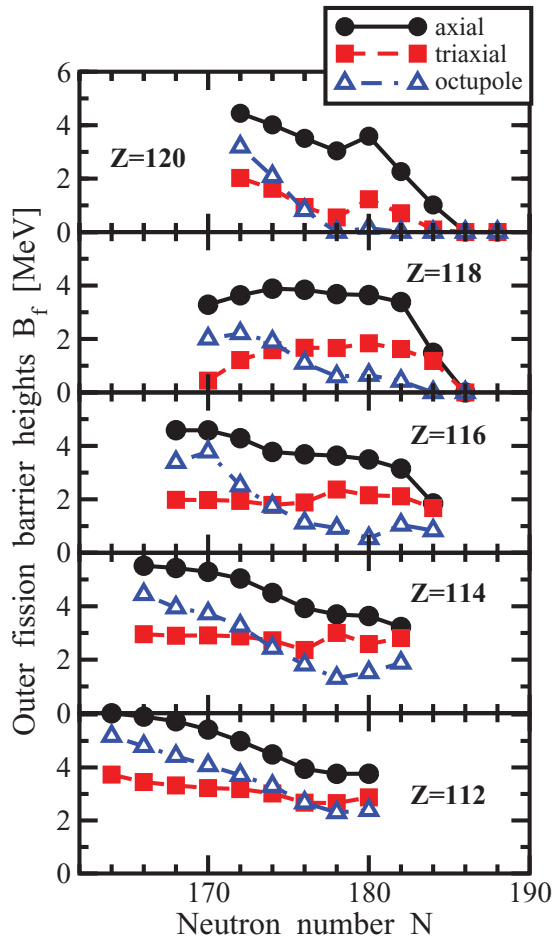
FIG. 10. (Color online) The heights of outer fission barriers of even-even $Z = 112$–120 nuclei relative to spherical or weakly (normal) deformed minima as a function of neutron number. The results of calculations of type A (axial), T (triaxial), and O (octupole) obtained with the NL3* parametrization are presented.

FIG. 11. (Color online) The same as in Fig. 5 but for the nuclei $^{298}120$ and $^{306}120$. Note that for simplicity only the axial solution (A) is shown at $\beta_2 < 0.5$.

are hard to compare because of the different spin-orbit force used in this model. We have, however, to keep in mind that triaxiality reduces the barriers in the actinides, but not in the superheavy elements with $Z = 112$, 114, and 116. Therefore, at the moment, we can only conclude that for a final comparison with the experimental data we have to wait for full RHB calculations or at least RMF + BCS calculations with the finite-range Gogny force in the pairing channel. Investigations in this direction are in progress.

It is well known that reflection-asymmetric (octupole deformed) shapes become important at the second fission barrier and beyond (see Refs. [2,7] and references therein). Our calculations indicate that triaxiality can play a similarly important role at the outer fission barriers. Usually, the triaxiality of these barriers is not mentioned in the publications. To our knowledge, it is only discussed in Ref. [6] that nonaxial degrees of freedom play an important role in the description of outer fission barriers of actinides. Figure 10 compares the energies of outer barrier saddle points as obtained in axial reflection-symmetric (A), triaxial (T), and axial reflection-asymmetric (octupole deformed) (O) calculations. One can see
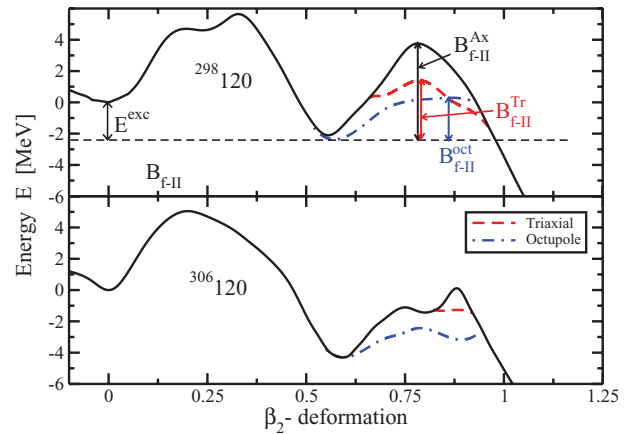
that the inclusion of triaxiality or octupole deformation always lowers the outer fission barrier. The underlying shell structure clearly defines which of the saddle points (triaxial or octupole deformed) is lower in energy. For example, the lowest saddle point is obtained in triaxial calculations in proton-rich nuclei ($N < 174$). In contrast, the lowest saddle point is obtained in octupole deformed calculations in neutron-rich nuclei ($N > 174$). Note that the decrease of the saddle-point energy by octupole deformation or triaxiality reaches 3 MeV in some nuclei. Thus, one can conclude that, due to the structure of the PES in the fission path valley, we observe in the superheavy region a situation opposite to that of actinide nuclei, where the triaxiality has no impact on the outer fission barriers. Our results also suggest that in some superheavy nuclei (mostly in the nuclei where the deformation energy curves of the A and O calculations are similar in energy) the combination of two deformations (triaxiality and odd-multipole deformations) may be important in the definition of the fission path for $\beta_2 \geqslant 0.5$. The CDFT calculations with both deformations included are at present not yet possible, but they require further investigations.

Figure 11 shows that some nuclei are superdeformed in the ground state. A summary for such nuclei is given in Table VIII. Whether these states are stable or metastable should be defined by the height and the width of the outer fission barrier. The current calculations show that in many nuclei this barrier is appreciable in the axial calculations of type A. However, the inclusion of triaxial or octupole deformation decreases this barrier substantially, so it is around 2 MeV in the majority of the nuclei. This low barrier would translate into a high penetration probability for spontaneous fission, such that most likely these superdeformed states are metastable. Calculations of the spontaneous fission half-lives from spherical or weakly deformed and superdeformed minima are needed in order to decide which of these minima is more stable against fission. Table VIII shows that the saddle point obtained in octupole deformed calculations (O) is the lowest in energy in most of the cases. Only in proton-rich $^{294}120$ and $^{290,292}118$ nuclei are the saddle points of triaxial calculations (T) the lowest.

TABLE VIII. A summary of the nuclei in which the superdeformed minimum is the lowest in energy. The energies of outer fission barrier saddle points with respect to this minimum, as obtained in axial (B_{f-II}^A), triaxial (B_{f-II}^T) and octupole (B_{f-II}^O) deformed calculations, are shown in columns 3, 4, and 5, respectively. For each nucleus, the outer saddle point with the lowest energy is shown in bold. The excitation energies E^{exc} of spherical or weakly (normal) deformed minima with respect to the superdeformed minima are shown in column 2. The graphical explanation of these quantities is also given in Fig. 11.

Nucleus	E^{exc}	B_{f-II}^A	B_{f-II}^T	B_{f-II}^O
1	2	3	4	5
		$Z = 120$ nuclei		
^{308}120	4.84	4.52	2.75	**1.62**
^{306}120	4.26	4.36	3.00	**1.82**
^{304}120	3.48	4.49	3.57	**2.07**
^{302}120	2.89	5.30	3.65	**2.55**
^{300}120	2.60	6.18	3.82	**2.61**
^{298}120	1.99	5.71	3.38	**2.25**
^{296}120	1.72	4.87	2.94	**2.52**
^{294}120	0.62	4.63	**2.24**	2.71
		$Z = 118$ nuclei		
^{304}118	2.68	2.41	2.14	**1.31**
^{302}118	2.92	3.58	2.42	**1.42**
^{300}118	1.78	5.16	3.40	**2.20**
^{298}118	1.70	5.34	3.54	**2.34**
^{296}118	1.48	5.17	3.15	**2.26**
^{294}118	1.15	4.99	2.82	**2.35**
^{292}118	0.69	4.58	**2.28**	2.59
^{290}118	0.40	4.03	**1.61**	2.60
		$Z = 116$ nuclei		
^{300}116	0.92	2.76	2.60	**1.75**
^{298}116	0.83	3.98	2.95	**1.88**

A superdeformed minimum exists also in the doubly magic nucleus ^{292}120 at a low excitation energy of approximately 0.6 MeV (see Fig. 5). This is definitely not an artifact of the model under consideration, since similar minima exist also in axial relativistic Hartree-Bogoliubov calculations with the DD-ME2 parametrization with Gogny D1S forces in the pairing channel (see Fig. 8 in Ref. [57]). Its calculated excitation energy depends on the actual strength of pairing and varies between 0 and 2 MeV.

It is interesting to compare our results for the structure of the outer fission barriers with those obtained in the axial RMF + BCS model (with and without reflection symmetry) of Ref. [52], in which the NL3 and NL-Z2 parametrizations were employed. Similar to our calculations, the superdeformed minima exist in the calculations of Ref. [52] (see Fig. 5 in this reference) without octupole deformation. However, in the calculations of Ref. [52] with the NL-Z2 parametrization, the heights of outer fission barriers with respect to the superdeformed minimum are lower by approximately 2 MeV compared to our calculations. As a consequence, the inclusion of octupole deformation completely eliminates the outer fission barriers, leading to results contradicting ours. On the other hand, the results of the calculations of Ref. [52] (see Fig. 6 in this reference) for a few selected nuclei based on
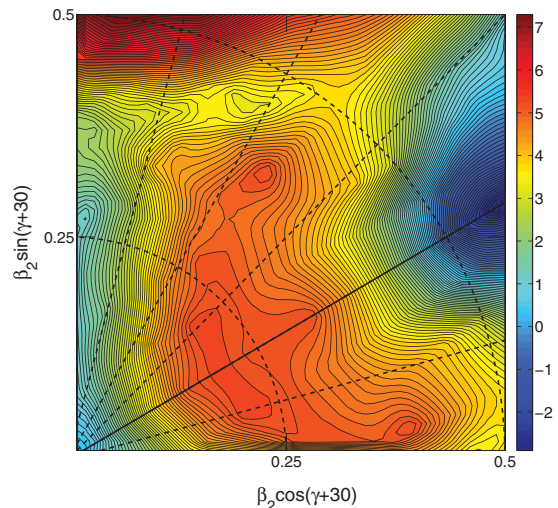

FIG. 12. (Color online) The same as in Fig. 4 but for the nucleus ^{302}120. In order to show the potential energy surface between the axial $\beta \sim 0.2$ and triaxial ($\beta_2 \sim 0.40$, $\gamma \sim 25°$) hills in greater detail the energy difference between two neighboring equipotential lines is set to 0.1 MeV and only one fourth of the deformation plane of Fig. 4 is shown.

the NL3 parametrization are very similar to ours; namely, the ground state is superdeformed and the outer fission barrier has a height of approximately 2.5 MeV. This result is not surprising given that the NL3* parametrization is very similar to NL3 [38]. However, the results of the calculations for a few selected $Z = 112$, 114, and 116 nuclei shown in Figs. 6 and 7 reveal that the outer fission barriers survive in the presence of octupole and triaxial deformation not only in the NL3* parametrization but also in the DD-ME2 and DD-PC1 parametrizations. On average, the height of the outer fission barrier in these nuclei is around 2 MeV. In contrast, the calculations with the NL-Z2 parametrization in Ref. [52] show that octupole deformation kills the outer fission barriers in these nuclei (see Fig. 5 in this reference).

IV. CONCLUSIONS

We have carried out systematic investigations of fission barriers in even-even superheavy nuclei with $Z = 112$–120 within covariant density functional theory including triaxial shapes with D2 symmetry and octupole shapes with axial symmetry. Three different classes of models with the state-of-the-art parametrizations NL3*, DD-ME2, and DD-PC1 were used in the calculations. Pairing correlations are taken into account in the BCS approximation using seniority pairing forces adjusted to empirical values of the gap parameters. The following conclusions have been obtained:

  (i) The low-Z and low-N nuclei in this region are characterized by axially symmetric inner fission barriers. The increase of the particle numbers leads to a softening of the potential energy surfaces in the triaxial plane. As a result, several competing fission paths in the region of the inner fission barrier emerge in some of the nuclei. Their importance in spontaneous fission

can be defined only by taking into account the fission dynamics more seriously. However, the results of the calculations within the macroscopic + microscopic method [67] suggest that the Tr-B path (and even maybe the Tr-A one) may not be so important since they are substantially longer compared with the axially symmetric path which leads to a significant reduction of the penetration probability.

  (ii) Triaxiality lowers the outer fission barriers by 1.5–3 MeV in reflection-symmetric calculations. In many nuclei the lowering due to triaxiality is even more important than the one due to octupole deformation, which is known to be important for the outer fission barriers and beyond from previous calculations (see Ref. [52] and references therein). The underlying shell structure clearly defines a triaxial (octupole) saddle that is lower in energy for proton-rich nuclei with $N < 174$ (neutron-rich nuclei with $N > 174$).
 (iii) On average, inner and outer fission barriers obtained for the NL3* and DD-PC1 parametrizations are similar. In contrast, the DD-ME2 parametrization produces barriers which are 1–1.5 MeV higher than the ones obtained with NL3* and DD-PC1.
 (iv) The superdeformed minimum is the lowest in energy in some of these nuclei. In the present calculations, the outer fission barriers with respect to these minima are about 2 MeV high. Both minima and barriers

are present in all three classes of the CDFT models. It has to be investigated, however, whether these superdeformed minima are stable with respects to more general deformations not taken into account so far.

The comparison of our results with those of nonrelativistic models clearly shows that CDFT predictions for the heights of inner fission barriers in the superheavy region with a seniority-zero pairing force still remain on the lower end among nuclear structure models used so far. Only axially symmetric calculations with the finite-range Gogny force D1S in the pairing channel can reproduce the estimates of the inner fission barrier heights of Ref. [68]. Given the uncertainties of these estimates, investigation of other experimental observables that strongly depend on fission barrier heights, especially fission half-lives and β- or electron capture delayed fission, is needed. Work in this direction is in progress.

[1] H. Abusara, A. V. Afanasjev, and P. Ring, Phys. Rev. C **82**, 044303 (2010).
[2] A. Staszczak, A. Baran, J. Dobaczewski, and W. Nazarewicz, Phys. Rev. C **80**, 014309 (2009).
[3] M. Warda, J. L. Egido, L. M. Robledo, and K. Pomorski, Phys. Rev. C **66**, 014310 (2002).
[4] P. Möller, A. J. Sierk, and A. Iwamoto, Phys. Rev. Lett. **92**, 072501 (2004).
[5] A. Sobiczewski and M. Kowal, Phys. Scr., T **125**, 68 (2006).
[6] A. Dobrowolski, K. Pomorski, and J. Bartel, Phys. Rev. C **75**, 024613 (2007).
[7] P. Möller, A. J. Sierk, T. Ichikawa, A. Iwamoto, R. Bengtsson, H. Uhrenholt, and S. Åberg, Phys. Rev. C **79**, 064304 (2009).
[8] A. Dobrowolski, B. Nerlo-Pomorska, K. Pomorski, and J. Bartel, Acta Phys. Pol. B **40**, 705 (2009).
[9] M. Kowal, P. Jachimowicz, and A. Sobiczewski, Phys. Rev. C **82**, 014303 (2010).
[10] A. K. Dutta, J. M. Pearson, and F. Tondeur, Phys. Rev. C **61**, 054303 (2000).
[11] M. Bender, K. Rutz, P.-G. Reinhard, J. A. Maruhn, and W. Greiner, Phys. Rev. C **58**, 2126 (1998).
[12] L. Bonneau, P. Quentin, and D. Samsoen, Eur. Phys. J. A **21**, 391 (2004).
[13] A. Staszczak, J. Dobaczewski, and W. Nazarewicz, Acta Phys. Pol. B **38**, 1589 (2007).
[14] J.-P. Delaroche, M. Girod, H. Goutte, and J. Libert, Nucl. Phys. A **771**, 103 (2006).
[15] M. Warda, Eur. Phys. J. A **42**, 605 (2009).
[16] R. Rodríguez-Guzmán, P. Sarriguren, L. M. Robledo, and J. E. Garcia-Ramos, Phys. Rev. C **81**, 024310 (2010).
[17] Z. P. Li, T. Nikšić, D. Vretenar, P. Ring, and J. Meng, Phys. Rev. C **81**, 064321 (2010).
[18] P. Ring, H. Abusara, A. V. Afanasjev, G. A. Lalazissis, T. Nikšić, and D. Vretenar, Int. J. Mod. Phys. E **20**, 235 (2011).
[19] W. Kohn and L. J. Sham, Phys. Rev. **137**, A1697 (1965).
[20] W. Kohn and L. J. Sham, Phys. Rev. **140**, A1133 (1965).
[21] *Extended Density Functionals in Nuclear Structure Physics*, Vol. 641 of Lecture Notes in Physics, edited by G. A. Lalazissis, P. Ring, and D. Vretenar (Springer-Verlag, Heidelberg, 2004).
[22] T. D. Cohen, R. J. Furnstahl, and D. K. Griegel, Phys. Rev. C **45**, 1881 (1992).
[23] W. Koepf and P. Ring, Nucl. Phys. A **493**, 61 (1989).
[24] A. V. Afanasjev and H. Abusara, Phys. Rev. C **81**, 014309 (2010).
[25] U. Hofmann and P. Ring, Phys. Lett. B **214**, 307 (1988).
[26] A. V. Afanasjev and P. Ring, Phys. Rev. C **62**, 031302(R) (2000).
[27] A. V. Afanasjev and H. Abusara, Phys. Rev. C **82**, 034329 (2010).
[28] R. Brockmann and H. Toki, Phys. Rev. Lett. **68**, 3408 (1992).
[29] F. Hofmann, C. M. Keil, and H. Lenske, Phys. Rev. C **64**, 034314 (2001).
[30] M. Serra, T. Otsuka, Y. Akaishi, P. Ring, and S. Hirose, Prog. Theor. Phys. **113**, 1009 (2005).
[31] S. Hirose, M. Serra, P. Ring, T. Otsuka, and Y. Akaishi, Phys. Rev. C **75**, 024301 (2007).
[32] T. Nikšić, D. Vretenar, P. Finelli, and P. Ring, Phys. Rev. C **66**, 024306 (2002).
[33] G. A. Lalazissis, T. Nikšić, D. Vretenar, and P. Ring, Phys. Rev. C **71**, 024312 (2005).
[34] T. Nikšić, D. Vretenar, and P. Ring, Phys. Rev. C **78**, 034318 (2008).

[35] X. Roca-Maza, X. Viñas, M. Centelles, P. Ring, and P. Schuck, Phys. Rev. C **84**, 054309 (2011).

[36] D. Vretenar, A. V. Afanasjev, G. A. Lalazissis, and P. Ring, Phys. Rep. **409**, 101 (2005).

[37] T. Nikšić, D. Vretenar, and P. Ring, Prog. Part. Nucl. Phys. **66**, 519 (2011).

[38] G. A. Lalazissis, S. Karatzikos, R. Fossion, D. Peña Arteaga, A. V. Afanasjev, and P. Ring, Phys. Lett. B **671**, 36 (2009).

[39] S. Typel and H. H. Wolter, Nucl. Phys. A **656**, 331 (1999).

[40] Y. K. Gambhir, P. Ring, and A. Thimet, Ann. Phys. (NY) **198**, 132 (1990).

[41] J. D. Walecka, Ann. Phys. (NY) **83**, 491 (1974).

[42] B. D. Serot and J. D. Walecka, Adv. Nucl. Phys. **16**, 1 (1986).

[43] J. Boguta and A. R. Bodmer, Nucl. Phys. A **292**, 413 (1977).

[44] G. A. Lalazissis, J. König, and P. Ring, Phys. Rev. C **55**, 540 (1997).

[45] B. A. Nikolaus, T. Hoch, and D. G. Madland, Phys. Rev. C **46**, 1757 (1992).

[46] W. Koepf and P. Ring, Phys. Lett. B **212**, 397 (1988).

[47] P. Ring and P. Schuck, *The Nuclear Many-Body Problem* (Springer-Verlag, Berlin, 1980).

[48] P. Möller and J. Nix, Nucl. Phys. A **536**, 20 (1992).

[49] RIPL-3 stands for the reference input parameter library of the International Atomic Energy Agency located at [http://www-nds.iaea.org/ripl3/], which for actinides is based on Ref. [69].

[50] J. Dudek, A. Majhofer, and J. Skalski, J. Phys. G **6**, 447 (1980).

[51] I. Muntian, Z. Patyk, and A. Sobiczewski, Acta Phys. Pol. B **32**, 691 (2001).

[52] T. Bürvenich, M. Bender, J. A. Maruhn, and P.-G. Reinhard, Phys. Rev. C **69**, 014307 (2004).

[53] M. Bender, K. Rutz, P.-G. Reinhard, and J. A. Maruhn, Eur. Phys. J. A **8**, 59 (2000).

[54] M. Samyn, S. Goriely, and J. M. Pearson, Phys. Rev. C **72**, 044316 (2005).

[55] P. Möller, J. R. Nix, and K. L. Kratz, At. Data Nucl. Data Tables **66**, 131 (1997).

[56] A. Staszczak, J. Dobaczewski, and W. Nazarewicz, Int. J. Mod. Phys. E **16**, 310 (2007).

[57] S. Karatzikos, A. V. Afanasjev, G. A. Lalazissis, and P. Ring, Phys. Lett. B **689**, 72 (2010).

[58] A. Baran, A. Bulgac, M. McNeil Forbes, G. Hagen, W. Nazarewicz, N. Schunck, and M. V. Stoitsov, Phys. Rev. C **78**, 014318 (2008).

[59] A. Staszack, M. Stoitsov, A. Baran, and W. Nazarewicz, Eur. Phys. J. A **46**, 85 (2010).

[60] P. Ring, Y. K. Gambhir, and G. A. Lalazissis, Comput. Phys. Commun. **105**, 77 (1997).

[61] A. V. Afanasjev, J. König, and P. Ring, Phys. Rev. C **60**, 051303(R) (1999).

[62] A. V. Afanasjev, P. Ring, and J. König, Nucl. Phys. A **676**, 196 (2000).

[63] W. E, W. Ren, and E. Vanden-Eijnden, J. Chem. Phys. **126**, 164103 (2007).

[64] D. Sheppard, R. Terrell, and G. Henkelman, J. Chem. Phys. **128**, 134106 (2008).

[65] D. G. Madland and P. Möller, Los Alamos National Laboratory unclassified report, LA-UR-11-11447, 2011.

[66] A. V. Afanasjev, T. L. Khoo, S. Frauendorf, G. A. Lalazissis, and I. Ahmad, Phys. Rev. C **67**, 024309 (2003).

[67] R. A. Gherghescu, J. Skalski, Z. Patyk, and A. Sobiczewski, Nucl. Phys. A **651**, 237 (1999).

[68] M. G. Itkis, Y. T. Oganessian, and V. I. Zagrebaev, Phys. Rev. C **65**, 044602 (2002).

[69] V. M. Maslov. *RIPL-1 Handbook*, TEXDOC-000 (International Atomic Energy Agency, Vienna, 1998), Ch. 5.